crystals

MDPI

Article

Microstructural Evolution and Thermal Stability of Long Period Stacking Ordered Phases in $Mg_{97}Er_2Ni_1$ and $Mg_{97}Er_2Zn_1$ Alloys

Jian Yin [1,2], Yushun Liu [2,*] and Guo-Zhen Zhu [2,*]

[1] Key Laboratory of Jiangxi Province for Modern Agricultural Equipment, School of Mechanical and Electrical Engineering, Jinggangshan University, Ji'an 343009, China; yinjian@jgsu.edu.cn
[2] Department of Mechanical Engineering, Manitoba Institute for Materials, University of Manitoba, Winnipeg, MB R3T 5V6, Canada
* Correspondence: liuy11@myumanitoba.ca (Y.L.); guozhen.zhu@umanitoba.ca (G.-Z.Z.)

Abstract: The influence of transition metals (Ni and Zn) on the formation, morphology, and thermal stability of long-period stacking ordered (LPSO) phases in $Mg_{97}Er_2N_{i1}$ and $Mg_{97}Er_2Zn_1$ alloys was investigated. In the as-cast state, both alloys consist of α-Mg and LPSO phases. Heat treatment at 540 °C for 20 h dissolves block-like and lamellar LPSO phases into the α-Mg matrix in the $Mg_{97}Er_2Zn_1$ alloy, with lamellar LPSO phases reprecipitating during subsequent cooling from 540 °C to 400 °C. Comparative analysis shows that Ni significantly enhances the thermal stability of the LPSO phase compared to Zn. Ni favors the formation of block-shaped LPSO phases, while Zn facilitates lamellar LPSO precipitation within the α-Mg matrix. The LPSO phase in the $Mg_{97}Er_2Ni_1$ alloy exhibits an exceptionally high melting temperature of 605 °C, the highest reported for an LPSO phase. Additionally, heat treatment at 500 °C for 100 h preserves the area fraction of the LPSO phase in the $Mg_{97}Er_2Ni_1$ alloy, and at 540 °C for 100 h, the LPSO grains grow without phase dissolution or structural transformation of their 18R-type configuration. These findings provide valuable insights into the role of alloying transition metal elements in controlling the stability and morphology of LPSO phases, offering pathways for tailoring the morphology of the LPSO phase in the Mg-based alloys.

Keywords: magnesium; Mg-Er-Ni; Mg-Er-Zn; long period stacking order phase (LPSO)

check for updates

Citation: Yin, J.; Liu, Y.; Zhu, G.-Z. Microstructural Evolution and Thermal Stability of Long Period Stacking Ordered Phases in $Mg_{97}Er_2Ni_1$ and $Mg_{97}Er_2Zn_1$ Alloys. *Crystals* **2024**, *14*, 1092. https://doi.org/10.3390/cryst14121092

Academic Editor: Heinz-Günter Brokmeier

Received: 3 December 2024
Revised: 14 December 2024
Accepted: 17 December 2024
Published: 19 December 2024

Copyright: © 2024 by the authors. Licensee MDPI, Basel, Switzerland. This article is an open access article distributed under the terms and conditions of the Creative Commons Attribution (CC BY) license (https://creativecommons.org/licenses/by/4.0/).

1. Introduction

Magnesium (Mg) alloys are widely valued for their lightweight nature and excellent specific strength, making them ideal for applications in aerospace, automotive, and biomedical fields [1–5]. Among Mg-based alloy systems, Mg-RE (rare earth metal) alloys are renowned for their high strength and excellent corrosion resistance [3,4]. The addition of transition metals (TMs, such as Zn, Ni, or Cu) [6–15] or aluminum (Al) [16–18] to Mg-RE alloys can result in the formation of a secondary phase with a long-period stacking ordered (LPSO) structure. The LPSO phase imparts Mg-RE-TM or Mg-RE-Al alloys with unique mechanical properties [19–23] and corrosion behaviors [15,24–30]. As secondary phases, the LPSO phases influence the mechanical and corrosion properties of Mg-RE-TM or Mg-RE-Al alloys through their structure, morphology, amount, and distribution.

The morphology of the LPSO phase, typically manifesting as block-like or lamellar shapes, is a critical factor influencing the mechanical and corrosion properties of Mg-based alloys. Mechanically, block-like LPSO phases distributed along grain boundaries promote isometric crystal grains, enhancing ductility, as observed in Mg-Gd-Er-Zn-Zr alloys, while lamellar LPSO phases within grain interiors form strip-shaped grains, improving strength [19]. In $Mg_{94}Y_3Ni_3$ (at%) alloys, block-shaped LPSO phases aligned along the extrusion direction support the alloys to achieve a tensile yield strength of up to 502 MPa [20]. Similarly, in Mg-Y-Zn alloys, the blocky LPSO phase strengthens the alloy through strong basal fiber texture and deformation kink bands [21]. In contrast, the lamellar LPSO phase

enhances ultimate tensile strength and elongation via kink deformation while simultaneously improving damping capacity and mechanical properties in Mg-Gd-Y-Zn-Zr-Nd alloys [22]. Regarding corrosion behavior, the continuous distribution of blocky LPSO phases with moderate volume fractions minimizes corrosion rates in Mg-Zn-Y alloys [25], and lamellar LPSO phases promote uniform corrosion, reducing rates in Mg-Gd-Zn-Zr alloys [26]. However, lamellar LPSO phases can increase corrosion rates in Mg-Gd-Ni alloys by raising the cathodic phase fraction [27]. Morphological changes in blocky phases, such as transitioning from a continuous network to disordered rods in Mg-7.2Y-2.8Ni alloys, raise degradation rates by 27% [28]. Similarly, in Mg-Er-Gd-Ni alloys, continuous blocky networks act as corrosion barriers, while streamlined LPSO phases weaken this effect [29]. In MgGd3Ni3 (at%) alloys, transforming continuous blocky LPSO phases into discontinuous rod-like and lamellar forms increases corrosion rates by 58.1%, driven by changes in corrosion pathways and increased galvanic corrosion sites [30]. These findings highlight the key role of LPSO morphology in optimizing the mechanical and corrosion performance of Mg-based alloys.

Heat treatment is an important strategy to tailor the formation and morphology of the LSPO phases [19,22,31–36]. Ding [34] demonstrated that in the $Mg_{96.32}Gd_{2.5}Zn_1Zr_{0.18}$ alloy, a heat treatment at 500 °C transformed $(Mg,Zn)_3Gd$ into blocky LPSO phases. Wang [19] reported a similar transformation of the $(Mg,Zn)_3(Gd,Er)$ phase at grain boundaries into blocky LPSO phases in as-cast Mg-Gd-Er-Zn-Zr alloys after heat treatment between 400 °C and 515 °C. Li [35] demonstrated that in the Mg-10Gd-3Y-1.2Zn-0.4Zr (wt%) alloy, heat treatment at 525 °C gradually dissolved blocky LPSO phases. Dang [22] showed that in the Mg-10Gd-2Y-1Zn-0.5Zr-0.2Nd (wt%) alloy, no LPSO phase formed after heat treatment at 540 °C for 4 h, but lamellar LPSO phases emerged during subsequent heat treatment at 450 °C for 10 h. Wu [36] observed that in a Mg-10Gd-1Zn-0.5Zr (wt%) alloy, solution treatment at 460 °C for 12 h eliminated the lamellar LPSO phase, forming blocky LPSO phases at grain boundaries. Further heat treatment at 500 °C for 12 h dissolved the blocky phases, and subsequent solution treatment at 420 °C for 1 h resulted in uniform lamellar LPSO phases within the α-Mg matrix. These findings also imply that thermal stability of the LPSO phase at elevated temperatures is crucial in determining the morphology of the LPSO phase during the heat treatment. Yin [10] obtained a highly stable blocky LPSO phase, which can hardly dissolve into the α-Mg matrix at 500 °C, by introducing Ni element into the Mg-Gd alloy, suggesting that the thermal stability of the LPSO phase strongly depends on Ni element. Liu [8] reported that a replacement of Ni for Zn in the $Mg_{94}Y_4Zn_2$ (at%) alloy resulted in an increase in the melting temperature of the LPSO phase from 547.5 °C to 571.1 °C, showing thermal stability enhancement for the LPSO phase. However, the underlying mechanism of how Ni or Zn affects the formation and thermal stability of the LPSO phase remains unclear.

Recently, Mg-Er-Ni alloys have garnered significant interest due to their high strength and rapid corrosion rate, making them promising candidates for fracture tools in the oil industry [37–40]. The mechanical properties and corrosion behaviors of Mg-Er-Ni alloys are strongly influenced by the morphology of the LPSO phase. Therefore, Mg-Er-Ni alloy was chosen as the material of study to compare with Mg-Er-Zn alloy, aiming to better understand how Ni and Zn influence the morphology of the LPSO phase during heat treatment, offering new insights into tailoring LPSO phase morphology.

2. Experimental Procedure

The $Mg_{97}Er_2Ni_1$ and $Mg_{97}Er_2Zn_1$ (at%) alloys were fabricated using pure magnesium (Mg), erbium (Er), nickel (Ni), and zinc (Zn), each with a purity exceeding 99.9 wt%. According to the weight ratio of the alloy composition, pure metal materials of Mg, Er, Ni, or Zn were prepared. After removing surface oxides from the pure metal materials, the metals were placed into a graphite crucible. Using high-frequency induction heating, the metals were melted and thoroughly mixed. The temperature was maintained at approximately 750 °C for 30 min, followed by natural cooling to room temperature in the graphite cru-

cible to obtain the as-cast alloy ingot. The samples, with dimensions of approximately 10 mm × 10 mm × 8 mm, were cut from the as-cast alloy ingot for heat treatment. The heat treatments were conducted in an argon-protected furnace.

X-ray diffraction (XRD; D8 Advance, Bruker AXS, Karlsruhe, Germany) was performed using monochromatic Cu Kα radiation for phase identification at a scanning speed of 10°/min. Scanning electron microscopy (SEM; FEI Quanta 200, Hillsboro, OR, USA), equipped with energy-dispersive spectroscopy (EDS; Oxford IE250X-Max50, Abingdon, Oxfordshire, UK), was used to analyze the microstructure and phase compositions. Transmission electron microscopy (TEM; FEI Tecnai G2 F20, Eindhoven, The Netherlands) was employed to identify the structure of the LPSO phase. Differential thermal analysis (DTA; Diamond TG/DTA, PerkinElmer, Shelton, CT, USA) was conducted at a heating rate of 10 °C/min to assess the thermal behavior of the alloys.

SEM samples were polished using SiC grinding paper and then etched for less than 10 s in a 4% nitric acid in ethanol solution before observation. Energy-dispersive spectroscopy (EDS) analysis was conducted using an acceleration voltage of 20 kV and a working distance of about 10 mm. TEM samples were prepared by wire-cutting the ingot into thin slices (~1 mm thick), mechanically grinding them to a thickness of ~100 µm, and then punching out 3 mm diameter disks from the pre-ground slices, which were then thinned using an ion beam for final preparation. The area fraction of the LPSO phase was evaluated by counting the number of pixels in the SEM images.

3. Results and Discussion

3.1. Dual-Phase Microstructure in As-Cast Alloys

Both as-cast $Mg_{97}Er_2Ni_1$ and $Mg_{97}Er_2Zn_1$ alloys exhibit the dual-phase microstructure, as confirmed by X-ray diffraction (XRD) and electron microscopy (EM) characterization. Figure 1 shows the XRD patterns of as-cast $Mg_{97}Er_2Ni_1$ and $Mg_{97}Er_2Zn_1$ alloys, with the peak presence corresponding to both α-Mg and LPSO phase. The corresponding SEM images and EDS results are shown in Figure 2, presenting dendrite-like α-Mg matrix (dark area) and interconnected networks of block-like LPSO phase (light area). The measured area fractions of block-like LPSO phases in the network were ~39% for the $Mg_{97}Er_2Ni_1$ alloy and ~18% for the $Mg_{97}Er_2Zn_1$ alloy.

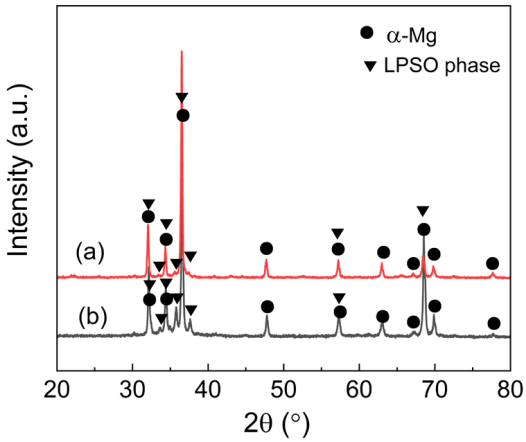


Figure 1. XRD patterns of as-cast (**a**) $Mg_{97}Er_2Ni_1$ and (**b**) $Mg_{97}Er_2Zn_1$ alloys.

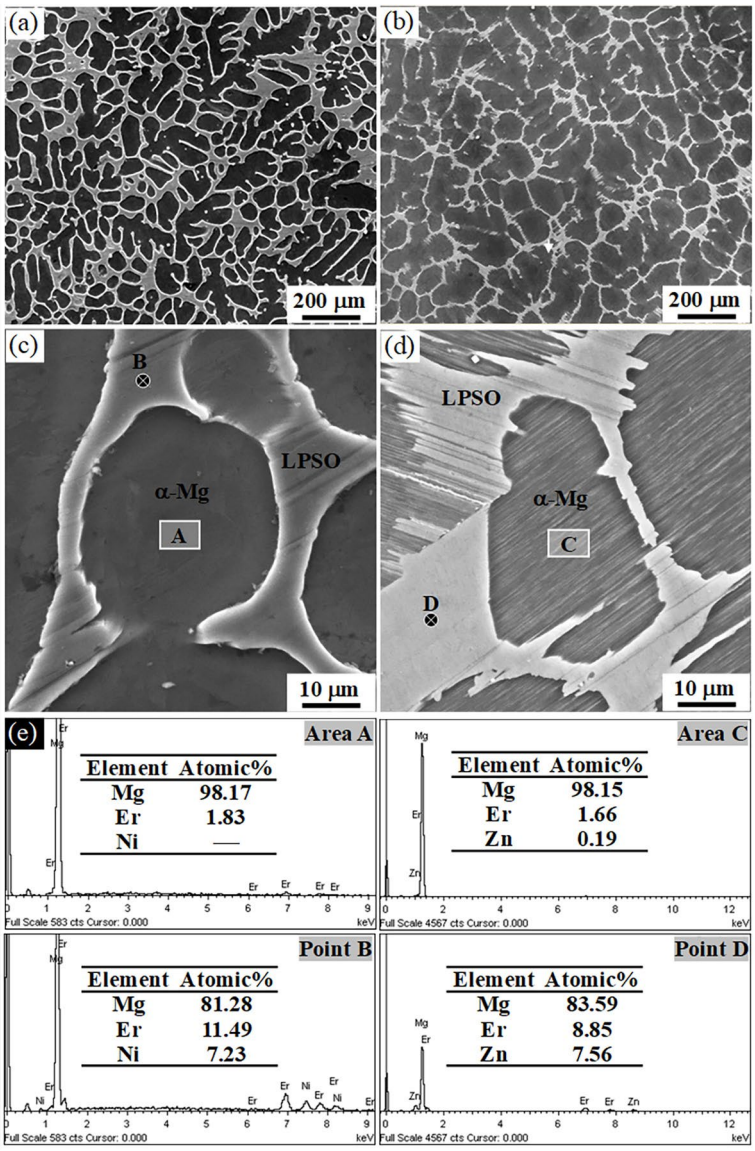


Figure 2. SEM images of the as-cast alloys: (**a**,**c**) $Mg_{97}Er_2Ni_1$ and (**b**,**d**) $Mg_{97}Er_2Zn_1$, along with (**e**) the corresponding EDS results.

Alongside interconnected networks of block-like LPSO phases, fine lamellar structures were observed within the α-Mg grains of the $Mg_{97}Er_2Zn_1$ alloy. These fine lamellar structures appear as needle-like features in light gray in Figure 2d, further supported by the corresponding EDX spectra shown in Figure 2e. The characteristics of lamellar LPSO phases embedded within the α-Mg grains suggest that the lamellar LPSO phase precipitates within the α-Mg grains during solidification. On the other hand, these lamellar structures were absent in the $Mg_{97}Er_2Ni_1$ alloy, as indicated by the morphology of Area A in Figure 2c and corresponding EDS results in Figure 2e, showing that no Ni element was detected in the α-Mg matrix.

It is known that the formation of LPSO structure requests the co-segregation of rare-earth (RE) elements and transition metals (TM, such as Ni or Zn) [6–15]. According to the Mg-Ni binary phase diagram, the maximum solid solubility of Ni in Mg is nearly zero across the temperature range from room temperature to 506 °C. In contrast, the Mg-Zn binary phase diagram shows a maximum solid solubility of Zn in Mg of 2.4 at% at 325 °C. As a result, during solidification, Ni atoms can be hardly incorporated into the α-Mg solid. This is consistent with the abovementioned fact that no Ni element was detected in the α-Mg matrix of the $Mg_{97}Er_2Ni_1$ alloy. However, Zn atoms could diffuse into α-Mg

and enable the formation of the LPSO phase within the α-Mg grains. This is evident by the morphology of the lamellar LPSO phase within the α-Mg grains of the $Mg_{97}Er_2Zn_1$ alloy shown in Figure 2d and the EDS result of the α-Mg grain (Mg-1.66 at%Er-0.19 at%Zn) in Figure 2e. This highlights a critical influence of the solubility of transitional metal elements in α-Mg on tailoring LPSO morphology, that is, Ni promotes block-like LPSO phase formation, while Zn enables both block-like and lamellae-like LPSO phases.

3.2. Thermal Stability of Involved LPSO Phases

The thermal behaviors of as-cast $Mg_{97}Er_2Ni_1$ and $Mg_{97}Er_2Zn_1$ alloys were investigated using differential thermal analysis (DTA), as shown in Figure 3. Both alloys exhibit two endothermic peaks. According to our previous study [10], the first peak corresponds to the melting of the LPSO phase, and the second one means the melting of the α-Mg phase. It is noted that the melting temperature of the LPSO phase in the $Mg_{97}Er_2Ni_1$ alloy is as high as 605 °C, which is 57 °C higher than that of the LPSO phase in the $Mg_{97}Er_2Zn_1$ alloy. This represents the highest melting temperature for an LPSO phase reported to date, significantly exceeding 528 °C for the LPSO phase in a Mg-Gd-Zn alloy [34], 550 °C for the LPSO phase in Mg-Y-Zn alloys [41], and 540 °C for the LPSO phase in Mg-Gd-Ni alloys [10].

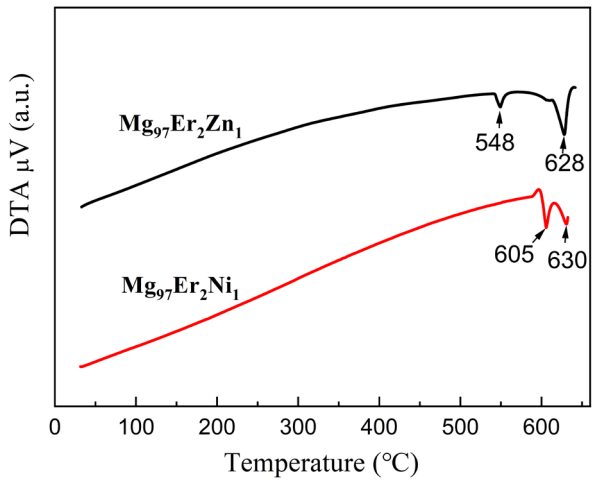


Figure 3. DTA curves of the as-cast $Mg_{97}Er_2Ni_1$ and $Mg_{97}Er_2Zn_1$ alloys.

The second peak, corresponding to the melting of α-Mg, is almost identical for both as-cast $Mg_{97}Er_2Ni_1$ and as-cast $Mg_{97}Er_2Zn_1$ alloys, suggesting that the RE and TM solutes have negligible influence on the melting of α-Mg. As the thermal analysis was conducted on the as-cast alloys, the phase transitions observed during heating can be considered the reverse process of solidification. During solidification, Mg enriched with RE and TM elements to its solubility limit initially precipitates as the dendritic α-Mg matrix from the molten liquid. It should be noted that Ni, which has very limited solubility in α-Mg, tends to stay exclusively in the remaining liquid, in contrast to Zn, which distributes between the α-Mg and the remaining liquid. The remaining liquid solidifies to form the LPSO phase between the α-Mg dendrites, resulting in a blocky LPSO network. In the meantime, within the α-Mg grains of as-cast $Mg_{97}Er_2Zn_1$ alloy, the lamellar LPSO phase precipitates as the presence of both Er and Zn. The thermal stability of LPSO phases and the speculated phase transitions were further examined by characterizing the microstructure and its evolution over the heat treatment temperatures ranging from 500 °C to 540 °C.

3.3. Microstructure Evolution During Heat Treatment

To investigate the microstructure evolution of $Mg_{97}Er_2Ni_1$ and $Mg_{97}Er_2Zn_1$ alloys during heat treatment, the as-cast alloys were subjected to heat treatments at temperatures near the phase transition ranges of typical LPSO phases. The two alloys were heat-treated at 540 °C for 20 h and then cooled down to 400 °C in the furnace, followed by quenching in the water.

Figure 4 presents the SEM images and corresponding EDS results of the heat-treated $Mg_{97}Er_2Ni_1$ and $Mg_{97}Er_2Zn_1$ alloys at 540 °C for 20 h. Compared to the as-cast alloy, the heat-treated $Mg_{97}Er_2Ni_1$ alloy is still composed of two phases of α-Mg and LPSO phase. The area fraction of the block-like LPSO phase is about ~37%, almost the same as the as-cast alloy; however, the morphology of the LPSO slightly changes, with the edges becoming more rounded. No Ni element was detected within the α-Mg matrix, as evidenced by the EDS result from Area A in Figure 4e. In contrast, the morphology of the LPSO phase has significant changes in the heat-treated $Mg_{97}Er_2Zn_1$ alloy, where the as-cast bulky LPSO phase network was broken. Enlarged SEM image (Figure 4d) and EDS result (Figure 4e) show that except for α-Mg and LPSO phases, there are Zn-rich particle phase formed, as illustrated by the black arrows in Figure 4d. Interestingly, no Zn was detected in α-Mg matrix, as evidenced by the composition of Mg-2.67 at%Er within Area E in α-Mg of the heat-treated $Mg_{97}Er_2Zn_1$ alloy. This suggests that during the heat treatment at 540 °C, Zn atoms tend to segregate into the LPSO phase or Zn-rich particle phase instead of α-Mg. Compared to the as-cast $Mg_{97}Er_2Zn_1$ alloy, no lamellar structure was observed in the α-Mg, as shown in Figure 4d, which should be attributed to the absence of Zn in the α-Mg matrix. This indicates that the heat treatment at 540 °C could enable the lamellar the LPSO phase to dissolve into the α-Mg matrix. In addition, the area fraction of the block-like LPSO phase in the heat-treated $Mg_{97}Er_2Zn_1$ alloy was measured to be ~9%, which is much less than ~18% for the as-cast $Mg_{97}Er_2Zn_1$ alloy. This suggests that the block-like LPSO phase in the $Mg_{97}Er_2Zn_1$ alloy is unstable and could dissolve into α-Mg.

Figure 5 shows the SEM images and corresponding EDS results of the $Mg_{97}Er_2Ni_1$ and $Mg_{97}Er_2Zn_1$ alloys cooled in the furnace to 400 °C after a heat treatment at 540 °C for 20 h. No obvious change was observed in the $Mg_{97}Er_2Ni_1$ alloy. However, in the $Mg_{97}Er_2Zn_1$ alloy, within the α-Mg grains, lamellar structure was observed, which suggests that the lamellar LPSO phase precipitates during the cooling from 540 °C to 400 °C. It is expected that upon cooling from 540 °C, the Zn atoms in the LPSO phase will diffuse into the α-Mg, enabling the formation of lamellar LPSO phase within α-Mg grains. As demonstrated above, a proper heat treatment could regulate not only the morphology of the LPSO phase but also its spatial distribution in the $Mg_{97}Er_2Zn_1$ alloy.

3.4. High Thermal Stability of LPSO Phase in a $Mg_{97}Er_2Ni_1$ Alloy

As indicated in the DTA analysis in Figure 2, the LPSO phase in the $Mg_{97}Er_2Ni_1$ alloy exhibits high thermal stability, corresponding to its phase transition temperature. To further confirm this, as-cast $Mg_{97}Er_2Ni_1$ samples were heat-treated at 500 °C and 540 °C for 100 h each.

Figure 6 compares the microstructures of the as-cast $Mg_{97}Er_2Ni_1$ alloy (denoted as the ACNi alloy), the alloy after heat treatment at 500 °C for 100 h (denoted as the 500Ni alloy), and the alloy after heat treatment at 540 °C for 100 h (denoted as the 540Ni alloy). The microstructure of the 500Ni alloy exhibits slight differences compared to the ACNi alloy, with both alloys showing nearly identical area fractions of the LPSO network (~39%). However, a detailed inspection of the enlarged SEM images in Figure 6b,d reveals that the edges of the LPSO phases in the 500Ni alloy are more rounded, suggesting that a degree of homogenization has occurred during the heat treatment at 500 °C.

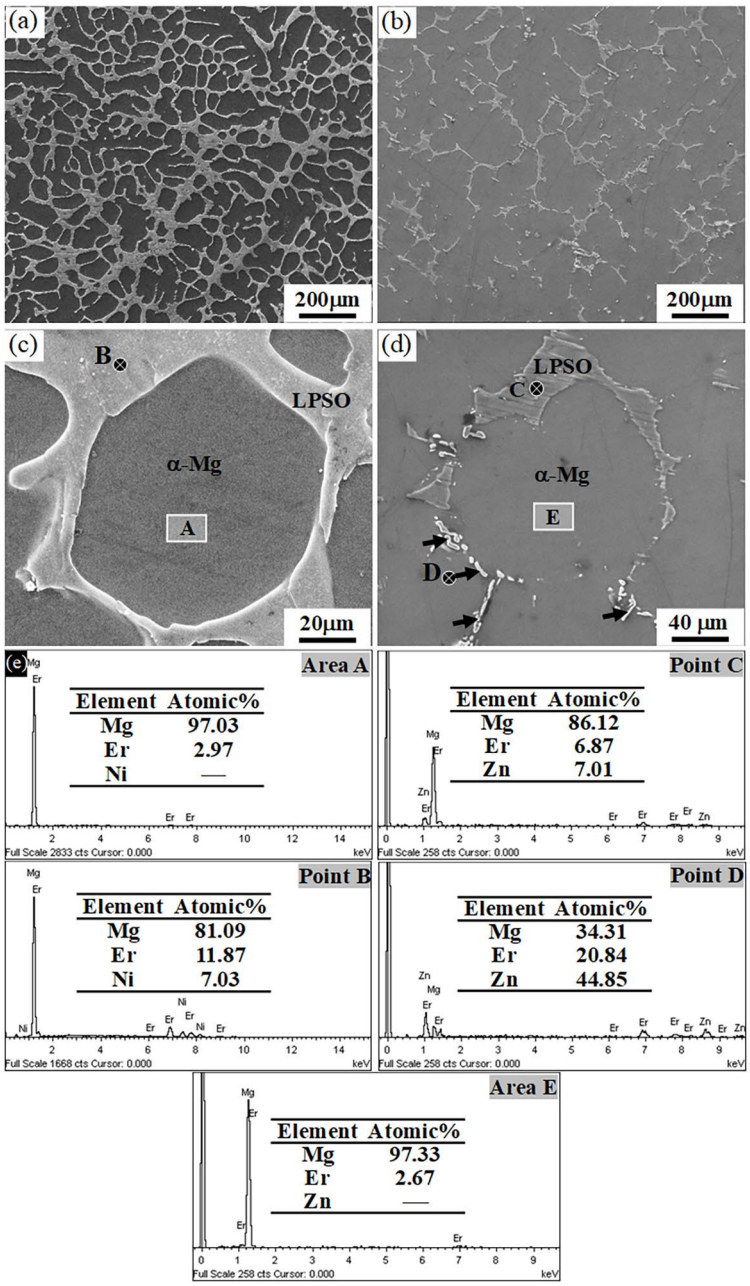


Figure 4. SEM images of (**a**,**c**) $Mg_{97}Er_2Ni_1$ and (**b**,**d**) $Mg_{97}Er_2Zn_1$ alloys after heat treatment at 540 °C for 20 h, along with (**e**) the corresponding EDS results.

In contrast, the microstructure of the 540Ni alloy shows significant changes compared to the ACNi and 500Ni alloys. Specifically, the number of thin LPSO network branches decreases markedly, and these thin branches are rarely observed in the 540Ni alloy. This indicates that the thinner LPSO structures are less stable at 540 °C. These observations suggest that the LPSO phase in the $Mg_{97}Er_2Ni_1$ alloy is relatively stable at 500 °C but undergoes noticeable change at 540 °C.

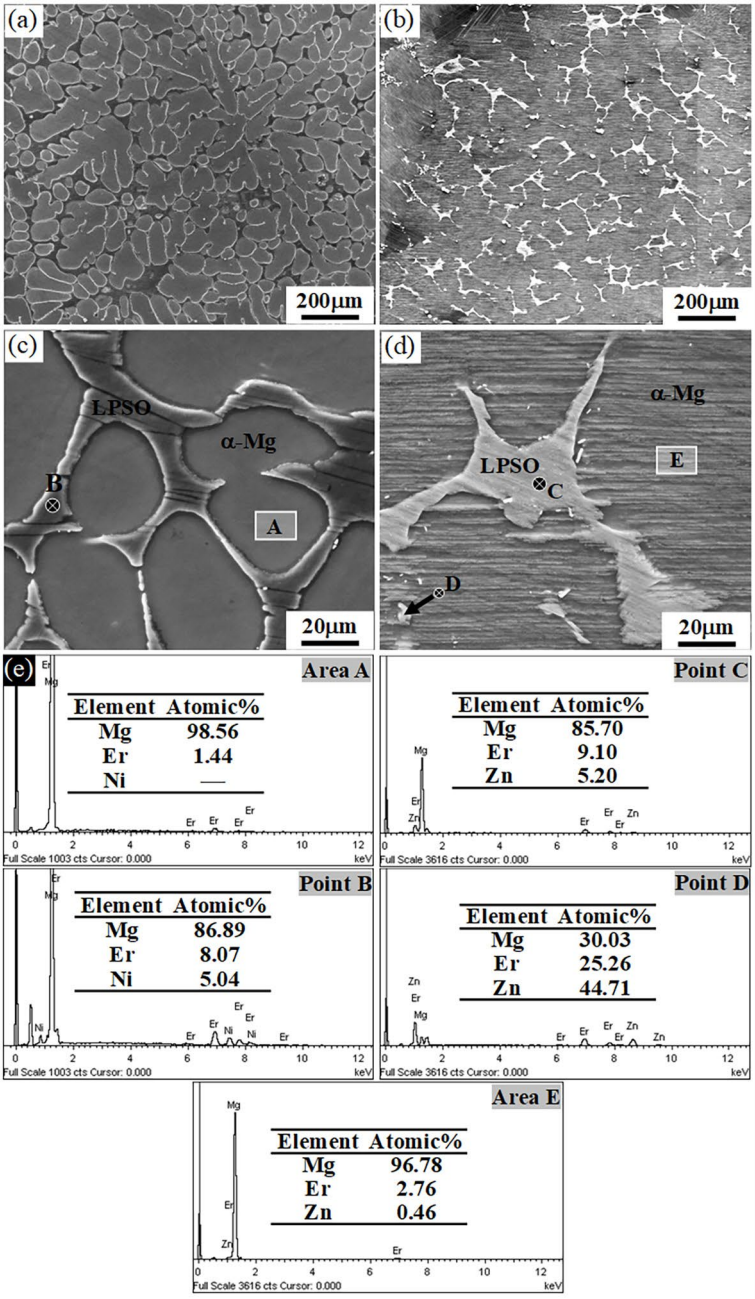


Figure 5. SEM images of (**a**,**c**) $Mg_{97}Er_2Ni_1$ and (**b**,**d**) $Mg_{97}Er_2Zn_1$ alloys after heat treatment at 540 °C for 20 h and subsequent furnace cooling to 400 °C followed by quenching in the water, along with (**e**) the corresponding EDS results.

The area fraction of the LPSO phase in the 540Ni alloy was measured to be ~36%, slightly lower than the ~39% observed for the ACNi and 500Ni alloys. This slight reduction in area fraction cannot be attributed to the dissolution of the LPSO phase into the α-Mg matrix. Figure 6g presents the EDS analysis of the 500Ni and 540Ni alloys, which indicates that no Ni was detected in the α-Mg matrix of either alloy, consistent with the results for the ACNi alloy shown in Figure 2e. This confirms that no Ni was dissolved into the α-Mg, and consequently, no LPSO phase dissolved into the matrix.

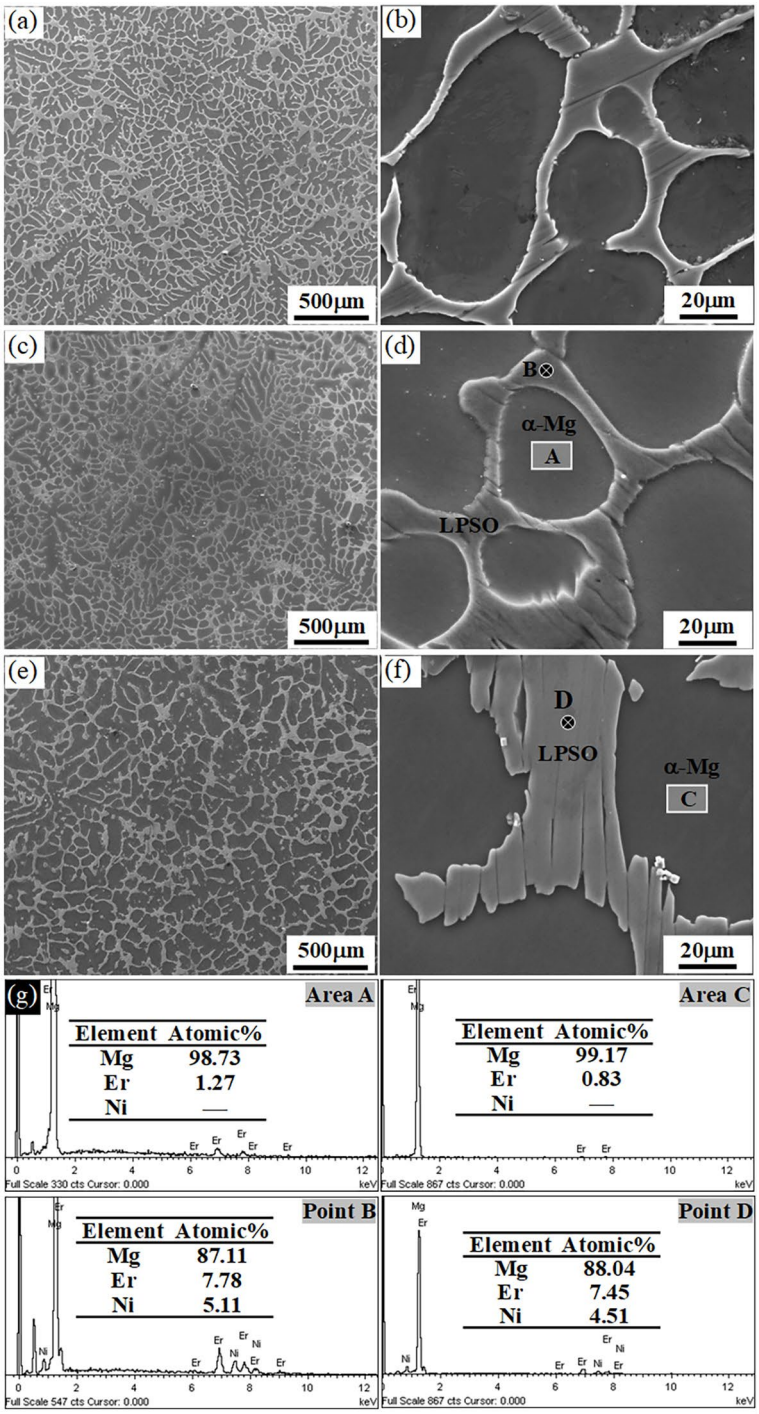


Figure 6. SEM images of $Mg_{97}Er_2Ni_1$ alloys: (**a**,**b**) in the as-cast condition, (**c**,**d**) after heat treatment at 500 °C for 100 h, and (**e**,**f**) after heat treatment at 540 °C for 100 h. The corresponding EDS results for the heat-treated alloys are presented in (**g**).

According to the Mg-Ni binary phase diagram, the eutectic temperature is 506 °C, and the solid solubility of Ni in Mg remains nearly zero from room temperature up to 506 °C. As a result, Ni atoms have very limited mobility and cannot easily diffuse into the α-Mg below 506 °C, which explains why the LPSO phase remains highly stable at 500 °C and why the thin LPSO branches persist even after 100 h of heat treatment.

Above 506 °C, however, Ni becomes more active and capable of diffusion. During heat treatment at 540 °C, this increased diffusion likely facilitates the growth of the LPSO phase. Thin LPSO branches may diffuse into adjacent LPSO structures, promoting their

thickening and coalescence. This phenomenon is supported by the observation in Figure 6e, where the LPSO network branches in the 540Ni alloy appear wider than those in the ACNi and 500Ni alloys. Therefore, the slight reduction in the area fraction of the LPSO phase in the 540Ni alloy compared to the ACNi alloy can be attributed to short-range diffusion within the LPSO structure, leading to its growth and redistribution. This also suggested a new way to tailor the morphology of the LPSO phase by controlling the diffusion of TM solutes at varying temperatures.

The LPSO structures in the ACNi and 540Ni alloys were analyzed using TEM. Figure 7 presents high-resolution TEM images and the corresponding SAED patterns along the $[11\bar{2}0]_{Mg}$ direction of the LPSO phases. In both TEM images, the atomic arrangement exhibits a periodic interval of approximately 1.57 nm, corresponding to six close-packed atomic layers. These layers form one of three six-layer building blocks (ABABCA) that make up the unit cell of the 18R structure [7]. The SAED patterns for both alloys reveal five extra diffraction spots positioned between the direct beam and the $(0002)_{Mg}$ reflection, characteristic of the 18R structure [7]. These observations confirm that the LPSO phase in both the ACNi and 540Ni alloys maintains an 18R configuration. The consistency in the structure between the two alloys indicates that heat treatment at 540 °C does not alter the type of LPSO phase in the $Mg_{97}Er_2Ni_1$ alloy.

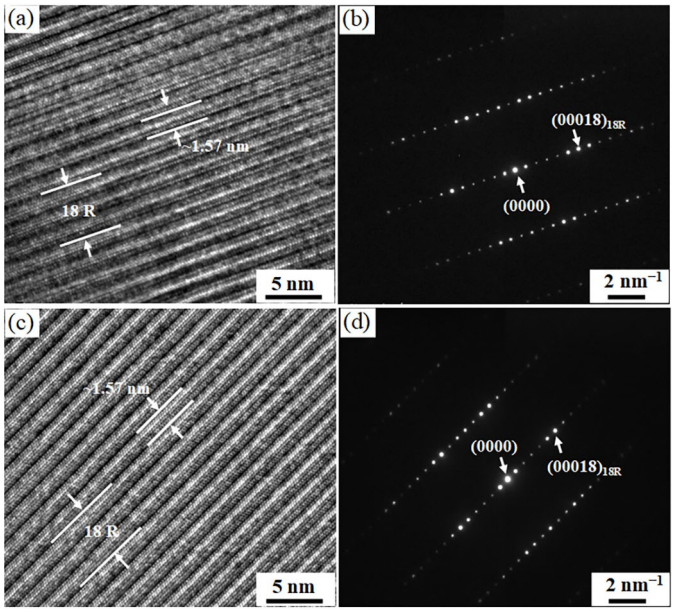


Figure 7. High-resolution TEM image and corresponding SAED pattern of the LPSO phase in the $Mg_{97}Er_2Ni_1$ alloys: (**a**,**b**) as-cast; (**c**,**d**) heat-treated alloys at 540 °C for 100 h. The electron beam is parallel to $[11\bar{2}0]$ of the α-Mg.

4. Conclusions

(1) In the as-cast state, both $Mg_{97}Er_2Ni_1$ and $Mg_{97}Er_2Zn_1$ alloys are composed of α-Mg and LPSO phases. Heat treatment at 540 °C for 20 h leads to the dissolution of both block-like and lamellar LPSO phases into the α-Mg matrix in the $Mg_{97}Er_2Zn_1$ alloy. During subsequent cooling from 540 °C to 400 °C, lamellar LPSO phases precipitate within the α-Mg grains.

(2) The LPSO phase in the $Mg_{97}Er_2Ni_1$ alloy exhibits an exceptionally high melting temperature of 605 °C, indicating superior thermal stability. After heat treatment at 500 °C for 100 h, the area fraction of the LPSO phase remains unchanged, underscoring its stability at 500 °C. At 540 °C, heat treatment promotes the growth of LPSO grains rather than dissolving the LPSO phase or altering its 18R-type structure. This indicates that elevated-temperature heat treatments can effectively modify the morphology of the LPSO phase without reducing its area fraction.

(3) Comparative heat treatment results demonstrate that Ni is more effective than Zn in enhancing the thermal stability of the LPSO phase. Ni promotes the formation of block-shaped LPSO phases, while Zn facilitates the precipitation of lamella-shaped LPSO phases within the α-Mg matrix, suggesting a way to tailor the morphology of the LPSO phase by adjusting the Ni or Zn elements.

These findings provide insights into the influence of alloying transition metal elements on the thermal stability and morphology of LPSO phases, offering potential pathways for tailoring the morphology of the LPSO phase in Mg-based alloys.

Author Contributions: The alloy samples were fabricated by J.Y.; the characterization was performed by J.Y. and Y.L.; data analysis was carried out by Y.L. and G.-Z.Z.; the manuscript was written by J.Y. and revised by Y.L. and G.-Z.Z. All authors have read and agreed to the published version of the manuscript.

Funding: J. Yin gratefully acknowledges the financial support of the National Natural Science Foundation of China (Grant No. 51661023) and the China Scholarship Council. Y. Liu and G.-Z. Zhu acknowledge the financial support of the NSERC Discovery Grant (RGPIN-2019-05882) and the Canada Research Chair program (CRC-2021-00512).

Data Availability Statement: The original contributions presented in this study are included in the article. Further inquiries can be directed to the corresponding author.

Conflicts of Interest: The authors declare no conflicts of interest.

References

1. Tan, J.; Ramakrishna, S. Applications of magnesium and its alloys: A review. *Appl. Sci.* **2021**, *11*, 6861. [CrossRef]
2. Kumar, L.G.S.; Thirumalaikumarasamy, D.; Karthikeyan, K.; Mathanbabu, M.; Ashokkumar, M.; Ramachandran, C.S. An overview of recent trends and challenges of post treatments on magnesium alloys. *Mater. Today Proc.* **2023**, *78*, 700–707. [CrossRef]
3. Wu, G.; Wang, C.; Sun, M.; Ding, W. Recent developments and applications on high-performance cast magnesium rare-earth alloys. *J. Magnes. Alloys* **2021**, *9*, 1–20. [CrossRef]
4. Zhang, J.; Liu, S.; Wu, R.; Hou, L.; Zhang, M. Recent developments in high-strength Mg-RE-based alloys: Focusing on Mg-Gd and Mg-Y systems. *J. Magnes. Alloys* **2018**, *6*, 277–291. [CrossRef]
5. Jayasathyakawin, S.; Ravichandran, M.; Baskar, N.; Chairman, C.A.; Balasundaram, R. Mechanical properties and applications of Magnesium alloy—Review. *Mater. Today Proc.* **2020**, *27*, 909–913. [CrossRef]
6. Geshani, M.S.; Kalayeh, P.M.; Asadi, A.H.; Mirzadeh, H.; Malekan, M.; Emamy, M. A review of Mg alloys containing long-period stacking ordered (LPSO) structures with insight into the application of friction stir processing. *J. Mater. Res. Technol.* **2023**, *24*, 4945–4966. [CrossRef]
7. Zhu, Y.M.; Morton, A.J.; Nie, J.F. The 18R and 14H long-period stacking ordered structures in Mg–Y–Zn alloys. *Acta Mater.* **2010**, *58*, 2936–2947. [CrossRef]
8. Liu, H.; Xue, F.; Bai, J.; Zhou, J.; Liu, X. Effect of substitution of 1 at% Ni for Zn on the microstructure and mechanical properties of $Mg_{94}Y_4Zn_2$ alloy. *Mater. Sci. Eng. A* **2013**, *585*, 387–395. [CrossRef]
9. Kawamura, Y.; Yamasaki, M. Formation and mechanical properties of $Mg_{97}Zn_1RE_2$ alloys with long-period stacking ordered structure. *Mater. Trans.* **2007**, *48*, 2986–2992. [CrossRef]
10. Yin, J.; Lu, C.; Ma, X.; Dai, B.; Chen, H.-L. Investigation of two-phase Mg-Gd-Ni alloys with highly stable long period stacking ordered phases. *Intermetallics* **2016**, *68*, 63–70. [CrossRef]
11. Liu, Y.; Yin, J.; Zhu, G. Solving Ambiguity in EBSD Indexing of Long-Period Stacking Ordered (LPSO) Phase in Mg with Template Matching Approach. *Crystals* **2024**, *14*, 932. [CrossRef]
12. Xu, H.; Jiang, J.; Bi, G.; Meng, S.; Zhang, X.; Li, Y.; Chen, T. Microstructure and mechanical properties of extruded and rolled Mg–Y–Zn–Ni–Co alloy. *J. Mater. Res. Technol.* **2023**, *27*, 8323–8333. [CrossRef]
13. Liu, H.; Huang, H.; Wang, C.; Sun, J.; Bai, J.; Xue, F.; Ma, A.; Chen, X.-B. Recent advances in LPSO-containing wrought magnesium alloys: Relationships between processing, microstructure, and mechanical properties. *JOM* **2019**, *71*, 3314–3327. [CrossRef]
14. Li, Y.; Yang, C.; Zeng, X.; Jin, P.; Qiu, D.; Ding, W. Microstructure evolution and mechanical properties of magnesium alloys containing long period stacking ordered phase. *Mater. Charact.* **2018**, *141*, 286–295. [CrossRef]
15. Xu, D.; Han, E.; Xu, Y. Effect of long-period stacking ordered phase on microstructure, mechanical property and corrosion resistance of Mg alloys: A review. *Prog. Nat. Sci. Mater. Int.* **2016**, *26*, 117–128. [CrossRef]
16. Zhu, Q.; Li, Y.; Zhang, H.; Wang, J.; Jiang, H.; Zhao, J. Revealing the Interaction between Dislocations and LPSO–Precipitates Structure in a Mg-Y-Al Alloy at Different Temperatures. *Crystals* **2024**, *14*, 1018. [CrossRef]
17. Kishida, K.; Yokobayashi, H.; Inui, H.; Yamasaki, M.; Kawamura, Y. The crystal structure of the LPSO phase of the 14H-type in the Mg–Al–Gd alloy system. *Intermetallics* **2012**, *31*, 55–64. [CrossRef]

18. Wang, Z.; Shen, Z.; Liu, Y.; Zhao, Y.; Zhu, Q.; Chen, Y.; Wang, J.; Li, Y.; Lozano-Perez, S.; Zeng, X. The effect of LPSO phase on the high-temperature oxidation of a stainless Mg-Y-Al alloy. *J. Magnes. Alloys* **2024**, *12*, 4045–4052. [CrossRef]
19. Wang, J.; Song, P.; Huang, S.; Pan, F. Effects of heat treatment on the morphology of long-period stacking ordered phase and the corresponding mechanical properties of Mg–9Gd–xEr–1.6 Zn–0.6 Zr magnesium alloys. *Mater. Sci. Eng. A* **2013**, *563*, 36–45. [CrossRef]
20. Wu, S.Z.; Qiao, X.G.; Qin, S.H.; Chi, Y.; Zheng, M. Improved strength in wrought Mg–Y–Ni alloys by adjusting the block-shaped LPSO phase and plate-shaped γ' phase. *Mater. Sci. Eng. A* **2022**, *831*, 142198. [CrossRef]
21. Yamasaki, M.; Hashimoto, K.; Hagihara, K.; Kawamura, Y. Effect of multimodal microstructure evolution on mechanical properties of Mg–Zn–Y extruded alloy. *Acta Mater.* **2011**, *59*, 3646–3658. [CrossRef]
22. Dang, C.; Wang, J.; Wang, J.; Yu, D.; Zheng, W.; Xu, C.; Lu, R. Effect of lamellar LPSO phase on mechanical properties and damping capacity in cast magnesium alloys. *J. Mater. Res. Technol.* **2023**, *22*, 2589–2599. [CrossRef]
23. Garces, G.; Barea, R.; Stark, A.; Schell, N. Anisotropic Plastic Behavior in an Extruded Long-Period Ordered Structure $Mg_{90}Y_{6.5}Ni_{3.5}$ (at.%) Alloy. *Crystals* **2020**, *10*, 279. [CrossRef]
24. Pałgan, D.; Dobkowska, A.; Zielińska, A.; Drozdenko, D.; Máthis, K.; Święszkowski, W. The Role of LPSO Structures in Corrosion Resistance of Mg-Y-Zn Alloys. *Crystals* **2022**, *12*, 1723. [CrossRef]
25. Zhang, J.; Xu, J.; Cheng, W.; Chen, C.; Kang, J. Corrosion behavior of Mg–Zn–Y alloy with long-period stacking ordered structures. *J. Mater. Sci. Technol.* **2012**, *28*, 1157–1162. [CrossRef]
26. Zhang, X.; Ba, Z.; Wang, Q.; Wu, Y.; Wang, Z.; Wang, Q. Uniform corrosion behavior of GZ51K alloy with long period stacking ordered structure for biomedical application. *Corros. Sci.* **2014**, *88*, 1–5. [CrossRef]
27. Ma, K.; Wang, J.; Peng, Y.; Dai, C.; Pan, Y.; Wang, D.; Wang, Y.; Pei, S.; Ma, Y. Enhanced degradation properties of Mg-Gd-Ni alloys by regulating LPSO morphology. *J. Phys. Chem. Solids* **2022**, *171*, 110974. [CrossRef]
28. Ma, K.; Wang, J.; Ren, J.; Dai, C.; Liu, S.; Peng, Y.; Pan, Y. Enhanced degradation properties of Mg-Y-Ni alloys by tailoring the LPSO morphology for fracturing tools applications. *Mater. Charact.* **2021**, *181*, 111489. [CrossRef]
29. Dai, C.; Zhang, S.; Wang, Y.; Wang, J.; Wang, J. Elucidation of the corrosion rate enhancement mechanism in Mg–Er–Gd–Ni alloys with high volume fraction of LPSO phase and different Gd contents after extrusion. *J. Mater. Res. Technol.* **2023**, *27*, 522–541. [CrossRef]
30. Dai, C.; Wang, J.; Pan, Y.; Ma, K.; Peng, Y.; Ren, J.; Wang, Y.; Wang, D.; Wang, J.; Ma, Y. Tailoring the microstructural characteristic and improving the corrosion rate of Mg-Gd-Ni alloy by heat treatment with different volume fraction of LPSO phase. *Corros. Sci.* **2023**, *210*, 110806. [CrossRef]
31. Li, Q.; Jin, L.; Wang, F.; Dong, S.; Zeng, J.; Wang, F.; Dong, J. Crack propagation path deflection induced by α-Mg/LPSO interface and its effect on the fracture toughness of cast Mg-RE-Zn alloys. *J. Magnes. Alloys* **2024**, *88*, 1–5. [CrossRef]
32. Zhang, G.; Niu, X.; Lu, R. Effects of heat treatment routes on microstructure and damping properties of Mg–Zn–Y–Mn alloys. *Mater. Res. Express* **2023**, *10*, 036515. [CrossRef]
33. Maier, P.; Schmahl, M.; Clausius, B.; Joy, C.; Fleck, C. Nanoindentation on the Transformation of LPSO Phases during Different Solution Heat Treatments in an Mg-Dy-Nd-Zn-Zr Alloy. *Crystals* **2022**, *12*, 1673. [CrossRef]
34. Ding, W.J.; Wu, Y.J.; Peng, L.M.; Zeng, X.; Yuan, G.; Lin, D. Formation of 14H-type long period stacking ordered structure in the as-cast and solid solution treated Mg-Gd-Zn-Zr alloys. *J. Mater. Res.* **2009**, *24*, 1842–1854. [CrossRef]
35. Li, D.; Zeng, X.; Dong, J.; Zhai, C. Influence of heat treatment on microstructure and mechanical properties of Mg-10Gd-3Y-1.2 Zn-0.4 Zr alloy. *Trans. Nonferrous Met. Soc. China* **2008**, *18*, s117–s121. [CrossRef]
36. Wu, X.; Pan, F.; Cheng, R.; Luo, S. Effect of morphology of long period stacking ordered phase on mechanical properties of Mg-10Gd-1Zn-0.5 Zr magnesium alloy. *Mater. Sci. Eng. A* **2018**, *726*, 64–68. [CrossRef]
37. Dai, C.; Wang, J.; Pan, Y.; Ma, K.; Peng, Y.; Wang, Y.; Wang, D.; Ran, C.; Wang, J.; Ma, Y. Achieving exceptionally high strength and rapid degradation rate of Mg-Er-Ni alloy by strengthening with lamellar γ' and bulk LPSO phases. *J. Mater. Sci. Technol.* **2024**, *168*, 88–102. [CrossRef]
38. Dai, C.; Pei, S.; Ma, K.; Wang, Y.; Wang, D.; Wang, J.; Ma, Y.; Wang, J. Rapid corrosion rates and high mechanical properties of as-extruded Mg–Er–Ni alloys by introducing LPSO and γ' phases. *J. Mater. Res. Technol.* **2023**, *24*, 6246–6263. [CrossRef]
39. Dai, C.; Pei, S.; Ma, K.; Wang, Y.; Wang, D.; Wang, J.; Ma, Y.; Wang, J. Revealing distinct corrosion mechanisms of soluble as-extruded Mg–Er–Ni alloy with LPSO and Mg_2Ni phase in different orientations. *J. Mater. Res. Technol.* **2023**, *26*, 1903–1921. [CrossRef]
40. Zhang, S.; Xie, X.; Ouyang, L.; Dai, C.; Li, H.; Xue, X.; Pei, S.; Wang, K.; Wang, J.; Pan, F. Thermo-mechanical processing characteristics and strain-rate-sensitive degradation properties of Mg-Er-Ni alloys. *J. Alloys Compd.* **2024**, *1004*, 175926. [CrossRef]
41. Chen, B.; Lin, D.; Zeng, X.; Lu, C. Effects of yttrium and zinc addition on the microstructure and mechanical properties of Mg–Y–Zn alloys. *J. Mater. Sci.* **2010**, *45*, 2510–2517. [CrossRef]

Disclaimer/Publisher's Note: The statements, opinions and data contained in all publications are solely those of the individual author(s) and contributor(s) and not of MDPI and/or the editor(s). MDPI and/or the editor(s) disclaim responsibility for any injury to people or property resulting from any ideas, methods, instructions or products referred to in the content.